Article

Fractal Operators Abstracted from Arterial Blood Flow

Tianyi Zhou [1], Yajun Yin [1],*, Gang Peng [2] , Chaoqian Luo [1] and Zhimo Jian [1]

[1] Department of Engineering Mechanics, Tsinghua University, Beijing 100084, China; zhouty20@mails.tsinghua.edu.cn (T.Z.); luocq19@mails.tsinghua.edu.cn (C.L.); jzm22@mails.tsinghua.edu.cn (Z.J.)

[2] Department of Civil Engineering, Chengdu Technological University, Chengdu 611730, China; pgang1@cdtu.edu.cn

* Correspondence: yinyj@tsinghua.edu.cn

Abstract: In this paper, we present a re-established functional fractal circuit model of arterial blood flow that incorporates the shunt effect of the branch vessels. Under the background of hemodynamics, we abstracted a family of fractal operators and investigate the kernel function and properties thereof. Based on fractal operators, the intrinsic relation between Bessel function and Struve function was revealed, and some new special functions were found. The results provide mathematical tools for biomechanics and automatic control.

Keywords: hemodynamics; functional circuit model; functional fractal space; fractal operator; kernel function; special function

1. Introduction

The functional circuit model (FCM) [1,2] is extensively employed in the field of hemodynamics. The arterial lumen can be considered as an elastic cavity with periodic contraction and dilation, known as the Windkessel model, introduced by Frank [2]. Based on the electrical-mechanical analogy, the blood flow movement within the elastic cavity can be simulated by a functional circuit model composed of basic electrical components. Frank's functional circuit model only involves a single elastic cavity and two components (a capacitor and a resistor), with limited simulation capabilities. Goldwyn et al. [3] proposed a multi-level elastic chamber model that incorporates the blood acceleration in space. Burattini et al. [4] and Stergiopulos et al. [5] introduced the inductive component to simulate the inertia of blood. With the increasement of the variety of electrical components and the number of cavities, more and more complex circuits were used to simulate blood flow movements more accurately [6–14].

Generally, the utilization of fluid dynamics methods based on the Navier–Stokes equations for simulating blood flow demands a substantial amount of computational resources and time due to high computation costs. In contrast, Windkessel models and FCM, which only require solving circuit equations without dealing with complex models and equations, can effectively simulate the pressure-flow relationship of hemodynamics at a relatively low computational cost, so they have been widely utilized and applied in medical diagnostics [15,16].

The concepts of fractal cells and fractal operators have been developed in recent years and successfully applied to various disciplines such as tendon and ligament, nerve, bone and hemodynamics [17–20]. The results indicate a close correlation between functional fractals and fractional dynamics. Based on the constitutive established by functional fractals, both fractional-order operators and fractional-order responses can be derived [21,22], which significantly differs from merely introducing fractional-order elements phenomenally [23–25]. In 2020, through the infinite-level division of the elastic cavities, Peng et al. [20] achieved the fractal of blood flow image and designed the functional fractal circuit of aorta and arterioles,

developing the hemodynamics in the functional fractal space. Recently, we realized that Peng's model ignored the shunt effect of branch vessels. Therefore, this paper enhances the model, establishing a new functional fractal circuit, and a family of fractal operators are abstracted from the new model. The properties of the operator family are studied. The study of operator properties is not limited to hemodynamics. In fact, since the circuits we have given are constructible with the components and parameters designable, the properties of the operators we have studied can serve as a foundation for automatic control and a better description of biological phenomena.

The present paper primarily encompasses the subsequent sections. In Section 2, the functional fractal circuit is established. In Section 3, the operator algebraic equations are established and solved. In Sections 4 and 5, the kernel functions of the fractal operator family are investigated.

2. Fractal Circuit Model

In the classical elastic cavity model (Windkessel model), the blood pressure P is compared to the voltage U, and the flow rate Q is compared to the current I. For the aorta, the longitudinal inertia of the blood flow is compared to the inductance L, causing the longitudinal flow; the wall compliance is compared to the capacitance C, causing the transverse flow. For the arteriole, transverse flow is also caused by the wall compliance, while the longitudinal flow is dominated by the blood viscosity, compared to the resistance R. the relationship between longitudinal and transverse flow can be likened to that of two branches in parallel of a circuit.

The comparative relationship between hemodynamics and the electric parameters is shown in Table 1. c_L and c_R are constant coefficients. r is the vessel radius, and h is the thickness of the vessel.

Table 1. The comparative correlation between parameters of hemodynamics and functional circuits [20,26].

Hemodynamic	Electric	Quantitative Correlation
Pressure P	Voltage U	$P = U$
Flow rate Q	Current I	$Q = I$
Blood inertia ρ	Inductance L	$L = c_L \rho / \left(\pi r^2 \right)$
Wall Compliance E	Capacitance C	$C = 3\pi r^2 / (2Eh)$
Blood Viscosity μ	Resistance R	$R = 8 c_R \mu / \left(\pi r^4 \right)$

Peng et al. [20] differentiated the classical single segment elastic cavity into a combination of infinite micro-elastic ones, which is inherited by this article as a basic thought. However, we notice that both the single elastic cavity model and Peng's infinite micro-elastic cavity model took no account of the branch vessels and therefore ignored the shunt effect of the branch vessels.

Nevertheless, the real artery has a multilevel branching topology, called "arterial vascular tree" in textbooks. Taking the aorta as an example, due to its numerous branch vessels, blood flowing through the aortic lumen continuously exits along these branches, forming tributaries. In this case, if we establish the elastic cavity model of the aorta, the shunt effect of tributaries should be taken into account.

When the shunt vessels are taken into account, the basic flow pattern of arterial blood flow can be described as follows, as depicted in Figure 1.

When the aortic wall undergoes contraction and dilation (indicated by black arrows in Figure 1), the blood flow within the vascular lumen exhibits three distinct patterns of flow (indicated by red arrows in Figure 1): axial (longitudinal) flow, radial (transverse) flow, and lateral branch flow. The axial flow is normal, that is, irrespective of whether the vessel wall dilates or contracts, axial flow always exists and maintains a consistent direction towards the distal end. There is a cooperative relationship between radial flow and branch flow, both driven by the motion of the vessel wall.
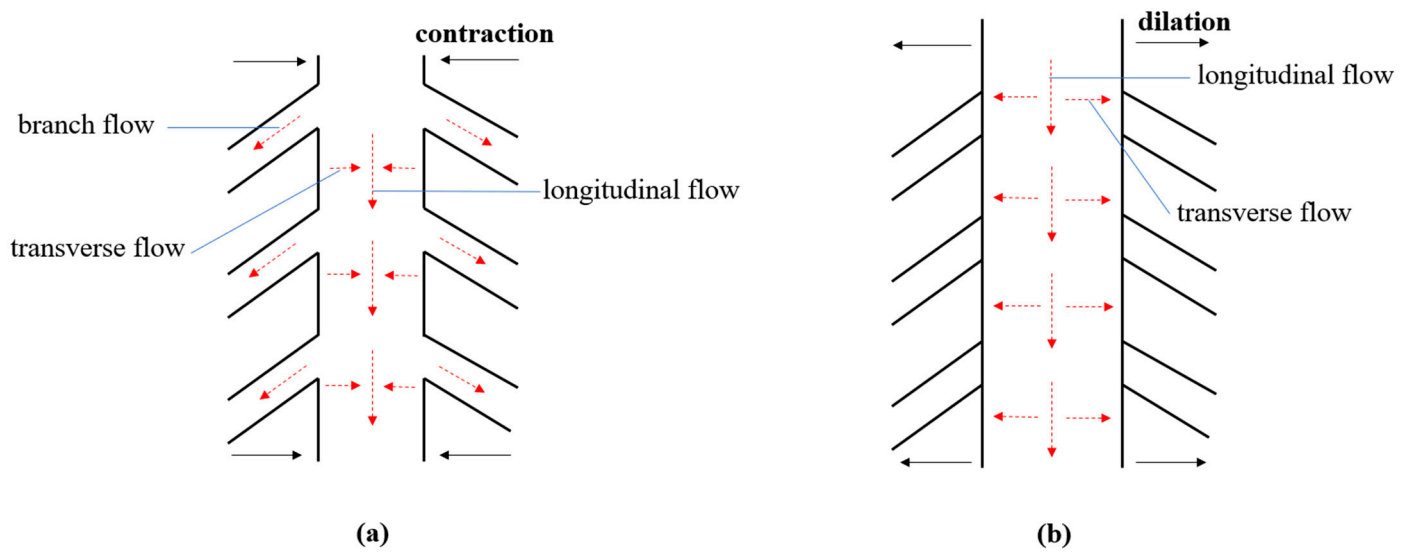
Figure 1. The basic pattern of arterial flow: (**a**) The arterial wall contracts. (**b**) The arterial wall dilates. There are three distinct patterns of flow: axial (longitudinal) flow, radial (transverse) flow, and the lateral branch flow, indicated by the red arrows. When the arterial wall contracts and dilates, the directions of the transverse flow are opposite. The direction of the longitudinal flow is constant. The branch flow exists when the arterial wall contracts. More details are explained in the content.

When the vessel wall contracts (indicated by the black arrows in Figure 1a), radial blood flow is directed from the wall towards the center (indicated by the red arrows in Figure 1a). Simultaneously, lateral branch flow is initiated, causing intracavity blood to exit the main cavity through branch blood vessels (indicated by the red arrows in Figure 1a). When the wall undergoes dilation (indicated by the black arrows in Figure 1b), radial blood flow is directed from the central region towards the wall (indicated by the red arrows in Figure 1b). Simultaneously, closure of the branch vessel channel occurs, effectively arresting branch flow and preventing any backflow of blood from the branch vessel into the main cavity.

According to the above flow patterns, the principal topological characteristics of arterial flow images can be summarized: for each micro-elastic cavity unit, the longitudinal (axial) flow in the main cavity is in parallel with the transverse (radial) flow; the blood flow in branch blood vessels runs parallel to that in the main vessel, and the branch blood flow of each micro-elastic cavity unit leads to infinity and no longer flows into the main blood vessel. By combining an infinite number of micro-elastic cavities, we can construct the functional fractal circuit shown in Figure 2. In Figure 2, M_1, M_2, and M_3 are basic electrical components, which could be inductors, capacitors, or resistors.

It could be seen that the functional fractal circuit in Figure 2 fully conforms to the mentioned topological characteristics of the blood flow image. Specifically, the parallel operation of M_1 and M_2 mirrors the parallel operation of the longitudinal and transverse blood flow; the branches of M_3 extend infinitely, corresponding to the branching outflow towards infinity, thereby becoming disconnected with the main vessel's blood flow.

Moreover, the functional fractal circuit in Figure 2 has the property of infinite self-similarity. The right side of Figure 2 gives the smallest repeating unit in the circuit, called the fractal cell. While classical fractals exhibit "self-similarity" [27,28], the functional fractal circuit demonstrates "self-congruence".
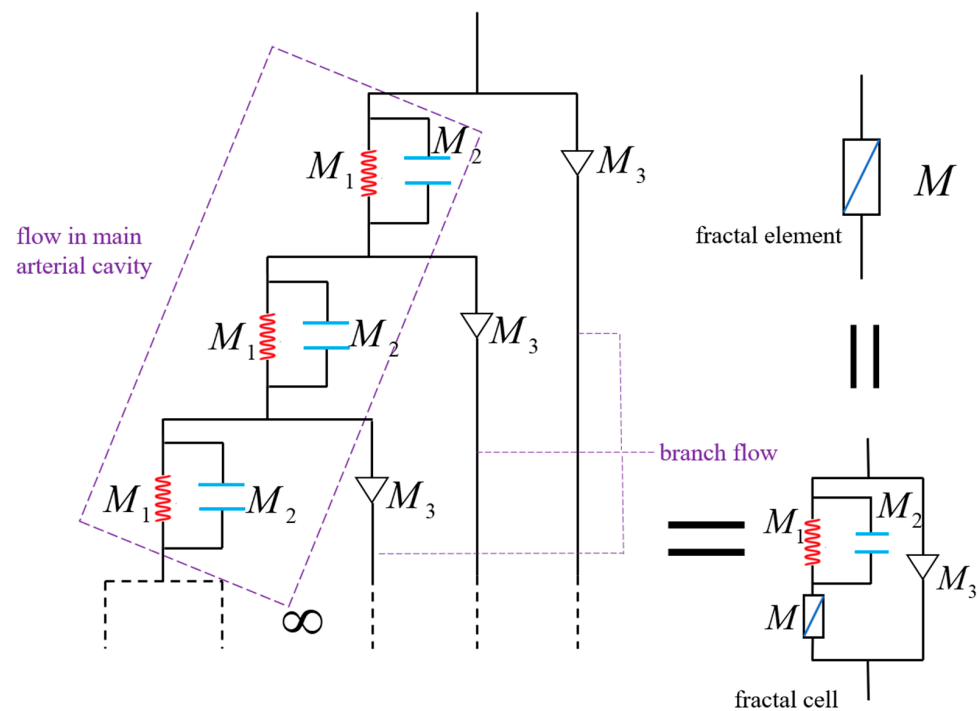
Figure 2. Functional fractal circuit and fractal cell. In the functional fractal circuit, electronic components M_1 and M_2 denote longitudinal and transverse flow in the main arterial cavity respectively, while M_3 denotes the flow in branch vessels. The right side gives the smallest repeating unit of the circuit, called the fractal cell.

It is noted that the flow patterns depicted in Figure 1 are universally observed in living organisms. Blood flow, lymph flow, and fluid flow in tissues can all be reduced to the movement patterns shown in Figure 1. In other words, the functional fractal shown in Figure 2 represents a spatial pattern with universal significance in biological systems. Therefore, the primary objective of this paper is not to investigate hemodynamics, but rather to examine the fundamental characteristics of functional fractal spaces utilizing blood flow images as a contextual backdrop. This approach offers a fresh perspective and establishes a novel mathematical foundation for studying fluid dynamics within living organisms.

3. Operator Algebraic Equations of the Fractal Circuit Model and Their Radical Solutions

According to Mikusinski's work [29], the basic differential and integral operators are defined as follows. If the function $f(t)$ has continuous derivatives at $t \geq 0$, then the definition of the differential operator acting on the function is

$$pf(t) = \frac{\mathrm{d}f(t)}{\mathrm{d}t} + f(0)\delta(t), \tag{1}$$

where $\delta(t)$ is the Dirac pulse function. The definition of integral operator l is that

$$lf(t) = \int_0^t f(\tau)\mathrm{d}\tau. \tag{2}$$

The definitions of the basic differential and integral operators p and l in this paper strictly adhere to the explicit forms presented in Mikusinski's work [29]. Based on basic differential operators and integral operators, Mikusinski constructed the operator domain, which is referred to as the Mikusinski operator field in this paper, and its internal structure has been described in detail in [29,30]. Mikusinski employed rigorous mathematical logic within his book to prove that the basic differential operator p and integral operator l defined by

(1) and (2) are mutually inverse, also demonstrating that their combined operation yields results independent of the order of action. In the Mikusinski operator field, Equation (3) is valid, which serves as a crucial logical foundation for operator algebra theory.

$$l = \frac{1}{p}. \tag{3}$$

Based on Equation (3), both differential operators and integral operators can be regarded as functions of the basic differential operator p defined in Equation (1).

Similar to Peng et al. [20], the admittance operator T is used to denote the map from voltage $u(t)$ to current $i(t)$, that is:

$$i(t) = Tu(t), \tag{4}$$

The concept of admittance is widely utilized in the field of electricity, and it serves as the reciprocal of impedance. Each electrical component has its corresponding admittance operator. Admittance operators for the three types of basic electrical components are presented in Table 2.

Table 2. Admittance operators for the three types of basic components [20].

Component	Admittance Operator	Note
Inductance L	$T_L = \frac{1}{Lp}$	First-order integral operator
Capacitance C	$T_C = Cp$	First-order derivative operator
Resistance R	$T_R = \frac{1}{R}$	Zero-order operator

The three admittance operators listed in Table 2 are all basic operators in the Mikusinski operator field.

In the functional fractal circuit shown in Figure 2, the admittance operators corresponding to the electrical components M_1, M_2, and M_3 are denoted as T_1, T_2, and T_3, respectively. The admittance operator of the fractal element M is denoted as T, referred to as the fractal operator. T_1, T_2, and T_3 are determined based on the selection of M_1, M_2, and M_3, respectively, according to Table 2. Therefore, T_1, T_2, and T_3 are operators in the Mikusinski operator field, which is a prerequisite for performing following algebraic operations on them.

The fractal cell in Figure 2 is equivalent to the entire fractal circuit, and the fractal circuit entirety is equivalent to a fractal element. Thus, it is immediately deduced that the fractal cell is equivalent to a fractal element. For the convenience of discussion, the equivalence is depicted in Figure 3, the admittance of each component or element denoted in parentheses.
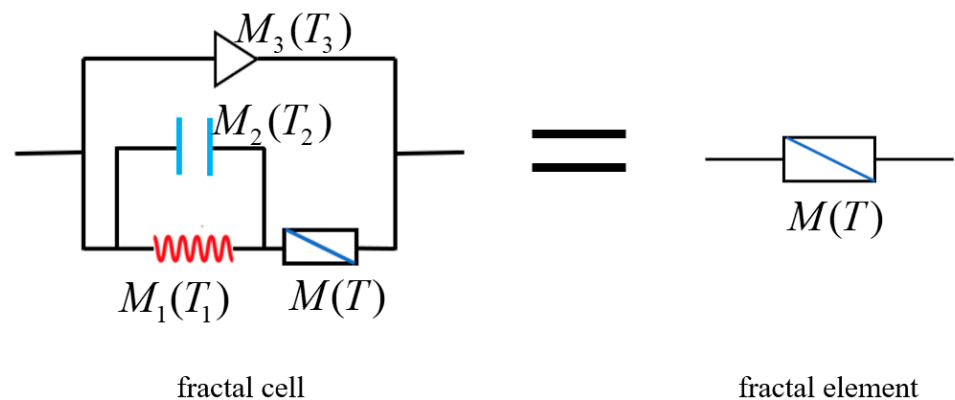

fractal cell   fractal element

Figure 3. The equivalence of the fractal cell and the fractal element.

Based on such equivalence and combined with operator algebra theory [29–32], the operator algebraic equation can be established:

$$\frac{(T_1 + T_2)T}{T_1 + T_2 + T} + T_3 = T. \tag{5}$$

The process of deriving Equation (5) is as follows: The parallel combination of M_1 and M_2 can be treated as a composite component with an admittance of $(T_1 + T_2)$. This composite component is then in series with the fractal element M, whose admittance is T, resulting in a total admittance of $\frac{(T_1+T_2)T}{(T_1+T_2)+T}$. Subsequently, the entire branch is in parallel with M_3, and their admittances are summed to obtain the overall admittance of the fractal cell, that is the left side of Equation (5). As the fractal cell is equivalent to the fractal element, their admittances are equal, thus ensuring that Equation (5) holds.

By rearranging Equation (5) we can obtain

$$T^2 - T_3 T - T_3(T_1 + T_2) = 0. \tag{6}$$

Equation (6) is the algebraic equation of the fractal operator T. It is a quadratic equation with one unknown, which has the radical solution

$$T = \frac{T_3 \pm \sqrt{T_3^2 + 4T_3(T_1 + T_2)}}{2}. \tag{7}$$

Since T_1, T_2, and T_3 are all functions of the basic differential operator p defined by Equation (1), the fractal operator T is also a function of p, i.e.,

$$T = T(p). \tag{8}$$

As introduced at the beginning of Section 2, the arteries are divided into the aorta and the arteriole, whose longitudinal flows are, respectively, dominated by inertia and viscosity. According to Table 1, the longitudinal flow of the aorta and the arteries are respectively denoted by the inductive component L and the resistive component R. The elasticity of the artery wall is represented by the capacitive component C. Therefore, as a direct application, M_1 and M_3 should be selected from the inductive L and the resistive R according to the type of main and branch vessels described, i.e., T_1 and T_3 should be selected from T_L and T_R; M_2 should be taken as the capacitive C, i.e., T_2 should be taken as T_C.

However, the discussion in this paper is not limited to this. The functional fractal circuit shown in Figure 2 provides a completely different topological structure than that of previous models, and the topological structure is universal in living bodies. Therefore, we hope to leverage the topological structure and optimize the control characteristics through different element matching methods, thereby obtaining valuable control results for the biomechanics and automatic control, not limited to hemodynamics. In the scope of this paper, the types of basic components are finite, so we can take an ergodic approach and discuss all possible cases where T_1, T_2 and T_3 take on admittance operators of various basic electronic components. These cases are constructible, and the components and parameter range are designable. See the analysis below for details.

Notice that there is a radical $\sqrt{(\cdot)}$ in the fractal operator. In the previous articles [21,22], we referred to the fractal operators with radical $\sqrt{(\cdot)}$ forms as fractional operators of apparent 1/2 order. Apparently, they are irrational fractional operators.

The fractal operator mentioned in Equation (7) is rooted in hemodynamics. It should be emphasized that the subjects and physical mechanisms studied in hemodynamics, ligament fiber mechanics, and nerve signal release dynamics are fundamentally distinct [33–37]. However, disciplines with such great differences have similar functional fractals, similar fractal operator algebraic equations, and similar radical operator solutions for algebraic equations. This means that it is imperative to study the radical operators uniformly.

The fractal operators in Equation (7) constitute a "family of fractal operators" of radical type. This raises a question: If we abandon the hemodynamic background and focus solely on investigating the fractal operator family, can we obtain results that hold universal significance? Specifically, we can ask the following question: How many basic or independent operators are there in the family of fractal operators? What are their properties? What are the similarities and differences between these properties? Clearly, by clarifying these questions, the toolbox of biomechanics and control theory can be greatly enriched.

There are three types of basic electrical components, resistance, inductance, and capacitance, as shown in Table 2. In Equation (7), there are exactly three operators, T_1, T_2, and T_3. Therefore, T_1, T_2, and T_3 can be selected as admittance operators of the three basic components respectively. By combining the three basic admittance operators, nine fractal operators can be obtained, as shown in Table 3.

Table 3. The family of fractal operators derived by the functional fractal circuit.

T_3	$T_1, T_2 = T_C, T_L$	$T_1, T_2 = T_C, T_R$	$T_1, T_2 = T_L, T_R$
T_R	$\frac{1}{2R}\left[1 \pm \sqrt{1 + 4RC\left(p + \frac{1}{LC}\frac{1}{p}\right)}\right]$	$\frac{1}{2R}\left[1 \pm \sqrt{5 + 4RCp}\right]$	$\frac{1}{2R}\left[1 \pm \sqrt{5 + \frac{4R}{L}\frac{1}{p}}\right]$
T_L	$\frac{1}{2L}\left[\frac{1}{p} \pm \sqrt{\frac{5}{p^2} + 4LC}\right]$	$\frac{1}{2L}\left[\frac{1}{p} \pm \sqrt{\frac{1}{p^2} + \frac{4L}{R}\frac{1}{p} + 4LC}\right]$	$\frac{1}{2L}\left[\frac{1}{p} \pm \sqrt{\frac{5}{p^2} + \frac{4L}{R}\frac{1}{p}}\right]$
T_C	$\frac{C}{2}\left[p \pm \sqrt{5p^2 + \frac{4}{LC}}\right]$	$\frac{C}{2}\left[p \pm \sqrt{5p^2 + \frac{4}{RC}p}\right]$	$\frac{C}{2}\left[p \pm \sqrt{p^2 + \frac{4}{RC}p + \frac{4}{LC}}\right]$

In Table 3, the powers of the basic differential operator p in the radical $\sqrt{(\cdot)}$, from -2 to 2, all appear. It can be said that Table 3 gives the basic graph of the $1/2$ order fractal operator.

All constants in Table 3 have specific physical significance: RC, LC, $\frac{L}{R}$, determining the characteristic frequency or characteristic time of a functional fractal system. In order to ensure the universality of the research results, we discard the specific meanings of the physical parameters, and then abstract the operators with radical $\sqrt{(\cdot)}$ into the following more general form: $\sqrt{p^2 + \alpha^2}$, $\frac{1}{p}\sqrt{p^2 + \alpha^2}$; $\sqrt{p + \alpha}$, $\frac{1}{p}\sqrt{p + \alpha}$, $\frac{1}{\sqrt{p}}\sqrt{p + \alpha}$; $\sqrt{(p + \beta)^2 - \alpha^2}$, $\frac{1}{p}\sqrt{(p + \beta)^2 - \alpha^2}$, $\frac{1}{\sqrt{p}}\sqrt{(p + \beta)^2 - \alpha^2}$. Without special instructions, we set $\alpha, \beta > 0$. α and β are physical constants that generally depends on the characteristic frequency or characteristic time.

4. Definition of Kernel Functions of Fractal Operators

The convolution of two functions $f(t)$ and $g(t)$ are defined as follows.

$$f(t) * g(t) \triangleq \int_0^t f(t - \tau)g(\tau)\mathrm{d}\tau. \tag{9}$$

According to Mikusinski's operator theory [29], as functions of the basic differential operator p, operators $T(p)$ can be defined by their kernel functions $K(t)$. Specifically, the action of operator $T(p)$ on a function $f(t)$ is equal to the convolution between the kernel function $K(t)$ of the operator $T(p)$ and the function $f(t)$, that is:

$$T(p)f(t) = K(t) * f(t) = \int_0^t K(t - \tau)f(\tau)\mathrm{d}\tau. \tag{10}$$

If we take $f(t)$ as the Dirac pulse function $\delta(t)$ from Equation (10), we can derive Equation (11).

$$T(p)\delta(t) = K(t). \tag{11}$$

Equation (11) means that, the kernel function (also called the integral kernel) of operator $T(p)$ is equal to the result of the action of $T(p)$ on the Dirac pulse function $\delta(t)$. As a direct definition of the kernel function, Equation (10) repeatedly is used in the remain part of the article.

Mikusinski did not provide a universal method for explicitly obtaining the kernel function of a general operator. Yu et al. [30], based on an analysis of the properties of the Minkusinsiki operator field and kernel function space, rigorously derived the following conclusion: when the definition of the basic differential operator p follows Equation (1), the kernel function $K(t)$ of the operator $T(p)$ can be obtained by taking the Laplace inverse transform of the operator function $T(p)$, that is:

$$\mathcal{L}^{-1}[T(p)] = K(t), \tag{12}$$

i.e.,

$$T(p)\delta(t) = K(t) = \mathcal{L}^{-1}[T(p)], \tag{13}$$

Based on the above theory, the kernel function of the fractal operator family can be clarified.

To solve differential equations, the Laplace transform on the differential equation is a well-known operation. Yu's work [30] rigorously demonstrated that within Mikusinski's operator algebra system, the integral kernel of an operator can be obtained by directly applying the Laplace inverse transform to the operator itself, eliminating the need for performing both Laplace transform and inverse transform on the entire differential equation. In fact, the operator solely encompasses the intrinsic properties of the system, whereas the differential equation incorporates both intrinsic information and external excitation (as depicted in (4)). Transforming the operator directly to obtain the integral kernel is more conducive to comprehending the inherent structure and properties of the system, which is exactly what we want in this paper.

5. Kernel Functions of the Fractal Operator Family

The present section focuses on the kernel functions of the exemplary fractal operators listed in Table 3.

5.1. Kernel Functions of the Fractal Operators $\sqrt{p^2 + \alpha^2}$ and $\frac{1}{p}\sqrt{p^2 + \alpha^2}$

Peng et al. [20] used to derive the operator $\sqrt{p^2 + \alpha^2} - p$ in hemodynamics. Mikusinski also discussed the operator in his work [29]. The inverse Laplace transformation of the fractal operator $\sqrt{p^2 + \alpha^2} - p$ is:

$$\mathcal{L}^{-1}\left(\sqrt{p^2 + \alpha^2} - p\right) = \frac{\alpha}{t}J_1(\alpha t), \tag{14}$$

where J_1 is the Bessel function of the first kind. As a direct application of Equation (12), the right side of Equation (14) gives the kernel function of the fractal operator $\sqrt{p^2 + \alpha^2} - p$. Thus, according to Equation (11) we have

$$\left[\sqrt{p^2 + \alpha^2} - p\right]\delta(t) = \frac{\alpha}{t}J_1(\alpha t). \tag{15}$$

The kernel function results given by Equations (14) and (15) are consistent with those obtained by Mikusinski [20] using a series expansion. Note that $\sqrt{p^2 + \alpha^2} - p$ is an irrational operator; therefore, its kernel is a non-elementary function, specifically a weighted Bessel function $\frac{\alpha}{t}J_1(\alpha t)$.

Based on Equation (15), we can analyze the operator $\frac{1}{p}\sqrt{p^2 + \alpha^2}$. Equation (13), combined with the inverse Laplace transformation, derives that

$$\mathcal{L}^{-1}\left(\frac{\sqrt{p^2 + \alpha^2} - p}{p}\right) = \int_0^t \frac{\alpha}{\tau} J_1(\alpha\tau)\mathrm{d}\tau, \tag{16}$$

So, the kernel function is

$$\begin{aligned}\left[\frac{\sqrt{p^2 + \alpha^2} - p}{p}\right]\delta(t) &= \int_0^t \frac{\alpha}{\tau} J_1(\alpha\tau)\mathrm{d}\tau \\ &= \frac{\alpha}{2}\{2[\alpha t J_0(\alpha t) - J_1(\alpha t)] + \pi\alpha t[J_1(\alpha t)H_0(\alpha t) - J_0(\alpha t)H_1(\alpha t)]\}\end{aligned} \tag{17}$$

The proof of the second equation of Equation (17) can be seen in Appendix A. H_0 and H_1 are zero-order and first-order Struve functions, respectively. $\frac{\sqrt{p^2 + \alpha^2} - p}{p}$ is an irrational operator, and its kernel function is a non-elementary function $\int_0^t \frac{\alpha}{\tau} J_1(\alpha\tau)\mathrm{d}\tau$. Curiously, the non-elementary function can be characterized by the Bessel function and the Struve function.

Figure 4 involves Bessel function $J_1(t)$, weighted Bessel function $\frac{J_1(t)}{t}$, and its integral $\int_0^t \frac{1}{\tau} J_1(\tau)\mathrm{d}\tau$. The graphs in Figure 4 demonstrate that all the three types of functions exhibit volatility, which evidently comes from the inherent properties of the Bessel function.
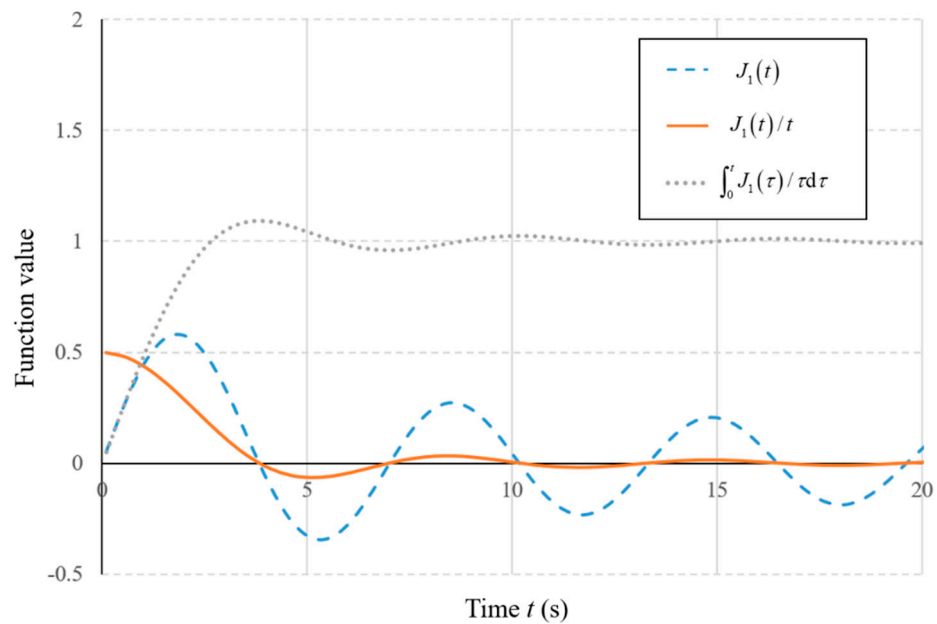

Figure 4. The graphs of three special classes of functions determined by the Bessel function.

As time tends to infinity, all three types of functions tend to converge towards a constant value, that is:

$$\lim_{t\to\infty} J_1(t) = \lim_{t\to\infty} \frac{J_1(t)}{t} = 0. \tag{18}$$

$$\lim_{t\to\infty} \int_0^t \frac{1}{\tau} J_1(\tau)\mathrm{d}\tau = 1. \tag{19}$$

Compared with the Bessel function $J_1(t)$, the weighted Bessel function $\frac{J_1(t)}{t}$ and its integral $\int_0^t \frac{1}{\tau} J_1(\tau)\mathrm{d}\tau$ exhibit a shorter convergence time to a constant value. Such superior convergence properties hold potential applications in the fields of biomechanics, biomimetic mechanics and automatic control.

Equation (17) is instructive. If the operator term on the left side of Equation (16) is discarded and only the second equation remains, it can be obtained that (see Appendix A for detailed proof):

$$\int_0^t \frac{1}{\tau}J_1(\alpha\tau)\mathrm{d}\tau = \frac{1}{2}\{2[\alpha t J_0(\alpha t) - J_1(\alpha t)] + \pi\alpha t[J_1(\alpha t)H_0(\alpha t) - J_0(\alpha t)H_1(\alpha t)]\}. \quad (20)$$

The Bessel function and the Struve function are associated by Equation (19). The Struve function arises from the nonhomogeneous Bessel equation given below [38]:

$$x^2\frac{\mathrm{d}^2 y}{\mathrm{d}x^2} + x\frac{\mathrm{d}y}{\mathrm{d}x} + \left(x^2 - m^2\right)y = \frac{4\left(\frac{x}{2}\right)^{m+1}}{\sqrt{\pi}\Gamma\left(m + \frac{1}{2}\right)}. \quad (21)$$

A set of solutions to the Equation (21) is

$$H_m(z) = \left(\frac{z}{2}\right)^{m+1}\sum_{n=0}^{\infty}\frac{(-1)^n\left(\frac{z}{2}\right)^{2n}}{\Gamma\left(n + \frac{3}{2}\right)\Gamma\left(n + m + \frac{3}{2}\right)}, \quad (22)$$

where $H_m(z)$ is the Struve function. Thus, Equation (19) is not particularly unexpected. Although there is a correlation between the Bessel function and the Struve function, what is really surprising is that they are correlated in such a complex way. It should be emphasized that they are very different special functions. Obviously, the irrational fractional operator $\frac{\sqrt{p^2+\alpha^2}-p}{p}$ serves as an exceptional bridge, connecting two distinct special functions in a remarkably ingenious manner.

The fractal operators have a clear biomechanical background, indicating that it is insufficient to describe the mechanical behavior of biological materials or structures solely through elementary functions. In practice, it is difficult to characterize the long-term behavior of organisms using elementary functions alone; non-elementary functions are necessary in such cases [39,40]. To a certain extent, it could be said that biomechanics is mechanics characterized by fractal operators and non-elementary functions.

As depicted in Figure 4, the kernel function of the fractal operator $\frac{\sqrt{p^2+\alpha^2}-p}{p}$ converges very fast and almost converges to a stable value after two oscillations. These desirable characteristics align perfectly with the requirements of automatic control theory. In particular, the parameters in the operator $\frac{\sqrt{p^2+\alpha^2}-p}{p}$ are designable. In other words, by designing the component parameters in the fractal circuit, we can obtain useful control characteristics.

5.2. Kernel Functions of the Fractal Operators $\sqrt{p^2 - \alpha^2}$ and $\frac{1}{p}\sqrt{p^2 - \alpha^2}$

Although operators $\sqrt{p^2 - \alpha^2}$ and $\frac{1}{p}\sqrt{p^2 - \alpha^2}$ do not appear in Table 3, they are deeply intrinsically related to the fractal operators $\sqrt{p^2 + \alpha^2}$ and $\frac{1}{p}\sqrt{p^2 + \alpha^2}$ in the above section, so they are also included in the family of radical type operators.

Introducing the fractal operator $\sqrt{p^2 - \alpha^2} - p$, there are two ways to obtain its kernel function. The first path is the inverse Laplace transformation. The inverse Laplace transformation of operator $\sqrt{p^2 - \alpha^2} - p$ gives that

$$\mathcal{L}^{-1}\left(\sqrt{p^2 - \alpha^2} - p\right) = -\frac{\alpha}{t}\bar{J}_1(\alpha t). \quad (23)$$

The function $-\frac{\alpha}{t}\bar{J}_1(\alpha t)$ at the right side of Equation (23) is the kernel function of the operator $\sqrt{p^2 - \alpha^2} - p$, where $\bar{J}_1(\alpha t)$ is the modified Bessel function of the first kind.

The second path is to consider a variable substitution. Extend the parameter α to a complex and introduce the complex transformation

$$\alpha \to i\alpha.$$

Then, the fractal operator $\sqrt{p^2 - \alpha^2} - p$ has the following transformation:

$$\sqrt{p^2 + \alpha^2} - p \to \sqrt{p^2 - \alpha^2} - p.$$

Thus, Equation (15) is transformed into

$$\left[\sqrt{p^2 - \alpha^2} - p\right]\delta(t) = \frac{i\alpha}{t}J_1(i\alpha t). \tag{24}$$

The transformation between the Bessel function $J_m(\alpha t)$ and the modified Bessel function $\bar{J}_m(\alpha t)$ is that

$$J_m(i\alpha t) = i^m \bar{J}_m(\alpha t). \tag{25}$$

The combination of Equations (22) and (23) immediately obtains Equation (26).

$$\left[\sqrt{p^2 - \alpha^2} - p\right]\delta(t) = -\frac{\alpha}{t}\bar{J}_1(\alpha t). \tag{26}$$

Similarly, Equation (16) is transformed into Equation (27).

$$\begin{aligned}
&\left[\frac{\sqrt{p^2 - \alpha^2} - p}{p}\right]\delta(t) = \int_0^t \frac{i\alpha}{\tau}J_1(i\alpha\tau)d\tau \\
&= \frac{i\alpha}{2}\{2[i\alpha t J_0(i\alpha t) - J_1(i\alpha t)] + \pi i\alpha t[J_1(i\alpha t)H_0(i\alpha t) - J_0(i\alpha t)H_1(i\alpha t)]\}
\end{aligned} \tag{27}$$

With the help of Equation (25), Equation (27) can be rewritten as Equation (28).

$$\begin{aligned}
&\left[\frac{\sqrt{p^2 - \alpha^2} - p}{p}\right]\delta(t) = -\int_0^t \frac{\alpha}{\tau}\bar{J}_1(\alpha\tau)d\tau \\
&= -\frac{\alpha}{2}\{2[\alpha t \bar{J}_0(\alpha t) - \bar{J}_1(\alpha t)] + \pi\alpha t[\bar{J}_1(\alpha t)iH_0(i\alpha t) - \bar{J}_0(\alpha t)H_1(i\alpha t)]\}
\end{aligned} \tag{28}$$

On the surface, Equation (27) is strange: the first equation exists in the field of real numbers, but the imaginary number appears in the last term of the second equation. However, further analysis reveals that this imaginary number can be eliminated. Based on the transformation between modified Struve function $\overline{H}_m(t)$ and Struve function $H_m(t)$:

$$H_m(it) = i^{m+1}\overline{H}_m(t), \tag{29}$$

$$\overline{H}_m(t) \triangleq \left(\frac{t}{2}\right)^{m+1} \sum_{n=0}^{\infty} \frac{\left(\dfrac{t}{2}\right)^{2n}}{\Gamma\left(n + \dfrac{3}{2}\right)\Gamma\left(n + m + \dfrac{3}{2}\right)}, \tag{30}$$

we can obtain

$$H_0(i\alpha t) = i\overline{H}_0(\alpha t), \tag{31}$$

$$H_1(i\alpha t) = -\overline{H}_1(\alpha t). \tag{32}$$

Then Equation (28) can be changed into

$$\left[\frac{\sqrt{p^2 - \alpha^2} - p}{p}\right]\delta(t) = -\int_0^t \frac{\alpha}{\tau}\bar{J}_1(\alpha\tau)\mathrm{d}\tau$$
$$= -\frac{\alpha}{2}\left\{2\left[\alpha t\bar{J}_0(\alpha t) - \bar{J}_1(\alpha t)\right] + \pi\alpha t\left[\bar{J}_0(\alpha t)\overline{H}_1(\alpha t) - \bar{J}_1(\alpha t)\overline{H}_0(\alpha t)\right]\right\} \tag{33}$$

That is, the kernel function of the fractal operator $\frac{\sqrt{p^2-\alpha^2}-p}{p}$ can be characterized by modified Bessel function and modified Struve function. Comparing Equations (33) and (17), fantastic symmetry can be seen. Discard the operator term and only retain the second equation of Equation (33), we obtain

$$\int_0^t \frac{1}{\tau}\bar{J}_1(\alpha\tau)\mathrm{d}\tau = \frac{1}{2}\left\{2\left[\alpha t\bar{J}_0(\alpha t) - \bar{J}_1(\alpha t)\right] + \pi\alpha t\left[\bar{J}_0(\alpha t)\overline{H}_1(\alpha t) - \bar{J}_1(\alpha t)\overline{H}_0(\alpha t)\right]\right\} \tag{34}$$

The modified Bessel function $\bar{J}_m(\alpha t)$ exhibits a profound intrinsic correlation with the modified Struve function $\overline{H}_m(\alpha t)$. Equations (34) and (20) still exhibit an elegant symmetry, which can be further enhanced as follows. The physical parameter α is present in both Equations (20) and (34). As mentioned earlier, α is the characteristic frequency of a functional fractal. However, mathematical theorems are typically independent of physics. To reveal the independence, the following variable substitution is introduced:

$$\alpha t \to t, \alpha\tau \to \tau.$$

Then, Equations (20) and (34) are transformed into the following forms, respectively:

$$\int_0^t \frac{1}{\tau}J_1(\tau)\mathrm{d}\tau = \frac{1}{2}\{2[tJ_0(t) - J_1(t)] + \pi t[J_1(t)H_0(t) - J_0(t)H_1(t)]\}. \tag{35}$$

$$\int_0^t \frac{1}{\tau}\bar{J}_1(\tau)\mathrm{d}\tau = \frac{1}{2}\left\{2\left[t\bar{J}_0(t) - \bar{J}_1(t)\right] + \pi t\left[\bar{J}_0(t)\overline{H}_1(t) - \bar{J}_1(t)\overline{H}_0(t)\right]\right\}. \tag{36}$$

The physical parameters disappear, and the symmetry is enhanced.

Comparing the content of this section with that of the previous section, it becomes evident that the entire theoretical system exhibits remarkable symmetry. The Bessel function $J_m(\alpha t)$ and the modified Bessel function $\bar{J}_m(\alpha t)$ demonstrate symmetrical characteristics. Similarly, the Struve function $H_m(\alpha t)$ and the modified Struve function $\overline{H}_m(\alpha t)$ also possess inherent symmetry. The symmetry arises from the symmetry between operators, that is, the structure of operator $\sqrt{p^2 + \alpha^2}$ and operator $\sqrt{p^2 - \alpha^2}$ are completely symmetric.

The graphs of modified Bessel function $\bar{J}_1(t)$, weighted modified Bessel function $\frac{\bar{J}_1(t)}{t}$, and its integral $\int_0^t \frac{1}{\tau}\bar{J}_1(\tau)\mathrm{d}\tau$ are shown in Figure 5. When time tends to zero, we obtain Equation (37).

$$\lim_{t\to 0}\bar{J}_1(t) = 0, \lim_{t\to 0}\frac{\bar{J}_1(t)}{t} = \frac{1}{2}, \lim_{t\to 0}\int_0^t \frac{1}{\tau}\bar{J}_1(\tau)\mathrm{d}\tau = 0 \tag{37}$$

That is, the values of the three types of special functions $\bar{J}_1(t)$, $\frac{\bar{J}_1(t)}{t}$, and $\int_0^t \frac{1}{\tau}\bar{J}_1(\tau)\mathrm{d}\tau$ remain finite at $t = 0$. When time tends to infinity, we obtain Equation (38).

$$\lim_{t\to\infty}\bar{J}_1(t) \to \infty, \lim_{t\to\infty}\frac{\bar{J}_1(t)}{t} \to \infty, \lim_{t\to\infty}\int_0^t \frac{1}{\tau}\bar{J}_1(\tau)\mathrm{d}\tau \to \infty. \tag{38}$$
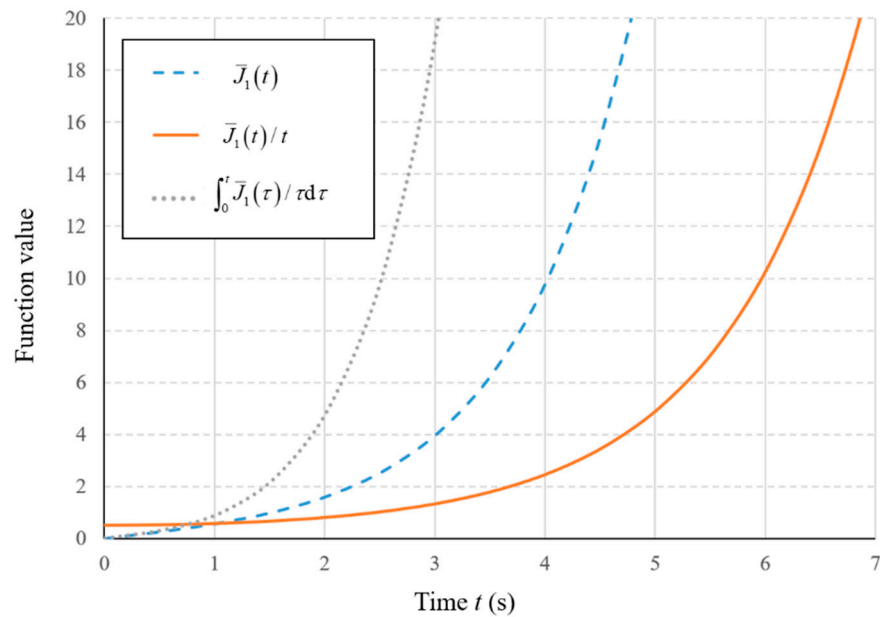
Figure 5. The graphs of three special classes of functions determined by the modified Bessel function.

That is, the three types of special functions all diverge, in which $\int_0^t \frac{1}{\tau}\bar{J}_1(\tau)d\tau$ demonstrates the fastest divergence rate, followed by $\bar{J}_1(t)$ and then $\lim_{t\to\infty}\frac{\bar{J}_1(t)}{t}$. It is evident that the divergence observed in the three types of functions stems from the inherent properties of the modified Bessel function.

Since the three kinds of special functions all diverge, the fractal operators $\left[\sqrt{p^2 - \alpha^2} - p\right]$ and $\left[\frac{\sqrt{p^2-\alpha^2}-p}{p}\right]$ and their kernel functions do not converge.

The theoretical and practical value of operators and functions that fail to converge is significantly constrained. How can we overcome these limitations? An effective method is as follows: mathematically, decay terms can be introduced into the kernel function; physically, the parameters of the physical components can be changed, introducing a translation into the operator. See the Section 5.3 for details.

5.3. Kernel Functions of the Fractal Operators $\sqrt{(p+\beta)^2 - \alpha^2}$, $\frac{1}{p}\sqrt{(p+\beta)^2 - \alpha^2}$ *and*

$\frac{1}{\sqrt{p}}\sqrt{(p+\beta)^2 - \alpha^2}$

In this section, the operators $\sqrt{(p+\beta)^2 - \alpha^2}$ and $\frac{1}{p}\sqrt{(p+\beta)^2 - \alpha^2}$ are considered. If we set $a = 0$, the two operators are reduced to the two operators $\sqrt{p^2 - \alpha^2}$ and $\frac{1}{p}\sqrt{p^2 - \alpha^2}$ in the previous section.

The direct acquisition of the kernel function of operators $\sqrt{(p+\beta)^2 - \alpha^2}$ and $\frac{1}{p}\sqrt{(p+\beta)^2 - \alpha^2}$ poses a challenge. However, we can take a detour. By combining operator $\sqrt{p^2 - \alpha^2}$ from the previous section with the translation transformation, operator $\sqrt{(p+\beta)^2 - \alpha^2}$ and its kernel function can be obtained.

By translation transformation, the operator p in Equation (23) is transformed into $p + a$:

$$p \to p + \beta,$$

Then the operator $\sqrt{p^2 - \alpha^2} - p$ is transformed into:

$$\sqrt{p^2 - \alpha^2} - p \to \sqrt{(p+\beta)^2 - \alpha^2} - (p+\beta).$$

Combined with the translation property of the Laplace transformation, we obtain

$$\mathcal{L}^{-1}\left[\sqrt{(p+\beta)^2-\alpha^2}-(p+\beta)\right]=-\frac{\alpha}{t}\overline{J}_1(\alpha t)e^{-\beta t}. \tag{39}$$

Then the kernel function of the fractal operator $\sqrt{(p+\beta)^2-\alpha^2}-(p+\beta)$ is

$$\left[\sqrt{(p+\beta)^2-\alpha^2}-(p+\beta)\right]\delta(t)=-\frac{\alpha}{t}\overline{J}_1(\alpha t)e^{-\beta t}. \tag{40}$$

From Equation (40), the kernel function of operator $\sqrt{(p+\beta)^2-\alpha^2}$ could be derived. Since $\sqrt{(p+\beta)^2-\alpha^2}$ is an irrational radical operator, its kernel is a non-elementary function. Notice that the decay term appears in the kernel function, specifically as the negative power exponential function $e^{-\beta t}$. If we let $\beta \to 0$ by translation transform, Equation (40) could be reduced to Equation (26).

When $t \to 0$, the limit of the kernel function $\frac{1}{t}\overline{J}_1(\alpha t)e^{-\beta t}$ is

$$\lim_{t\to 0}\left[\frac{1}{t}\overline{J}_1(\alpha t)e^{-\beta t}\right]=\frac{\alpha}{2}. \tag{41}$$

When $t \to \infty$, the limit of the kernel function $\frac{1}{t}\overline{J}_1(\alpha t)e^{-\beta t}$ should be discussed in two cases. In the case of $0 < \frac{\beta}{\alpha} < 1$, there is

$$\lim_{t\to \infty}\left[\frac{1}{t}\overline{J}_1(\alpha t)e^{-\beta t}\right]=\infty. \tag{42}$$

While in the case of $\frac{\beta}{\alpha} \geq 1$, there is

$$\lim_{t\to \infty}\left[\frac{1}{t}\overline{J}_1(\alpha t)e^{-\beta t}\right]=0. \tag{43}$$

Obviously, $\frac{\beta}{\alpha}=1$ is exactly the turning point of the monotonicity, the detailed analysis as follows. Suppose α is fixed as $\alpha = 1$, and the graphs of the kernel function $\frac{1}{t}\overline{J}_1(t)e^{-\beta t}$ with different values of *a* are shown in Figure 6. As shown in Figure 6, the convergence of the operator $\sqrt{(p+\beta)^2-\alpha^2}-(p+\beta)$ when $t \to \infty$ is determined by the value of $\frac{\beta}{\alpha}$. In the case of $0 < \frac{\beta}{\alpha} < 1$, the kernel function exhibits a decrement followed by an increment, ultimately tending towards infinity. In the case of $\frac{\beta}{\alpha}=1$, the function exactly loses its capability to increase. Evidently, in the case of $\frac{\beta}{\alpha} \geq 1$, the convergence of the kernel function $\frac{1}{t}\overline{J}_1(\alpha t)e^{-\beta t}$ in this section is much better than that of the non-convergent kernel function $\frac{1}{t}\overline{J}_1(\alpha t)$ in the previous section. It can be seen that in this case, the modulation effect of the negative power exponential function $e^{-\beta t}$ is highly significant, facilitating the transformation of a non-convergent kernel function $\frac{1}{t}\overline{J}_1(\alpha t)$ into a rapidly convergent one $\frac{1}{t}\overline{J}_1(\alpha t)e^{-\beta t}$.

For the operator $\frac{\sqrt{(p+\beta)^2-\alpha^2}-(p+\beta)}{p}$, Equation (38) combined with the inverse Laplace transform obtains

$$\mathcal{L}^{-1}\left[\frac{\sqrt{(p+\beta)^2-\alpha^2}-(p+\beta)}{p}\right]=-\int_0^t\frac{\alpha}{\tau}\overline{J}_1(\alpha\tau)e^{-\beta\tau}d\tau. \tag{44}$$
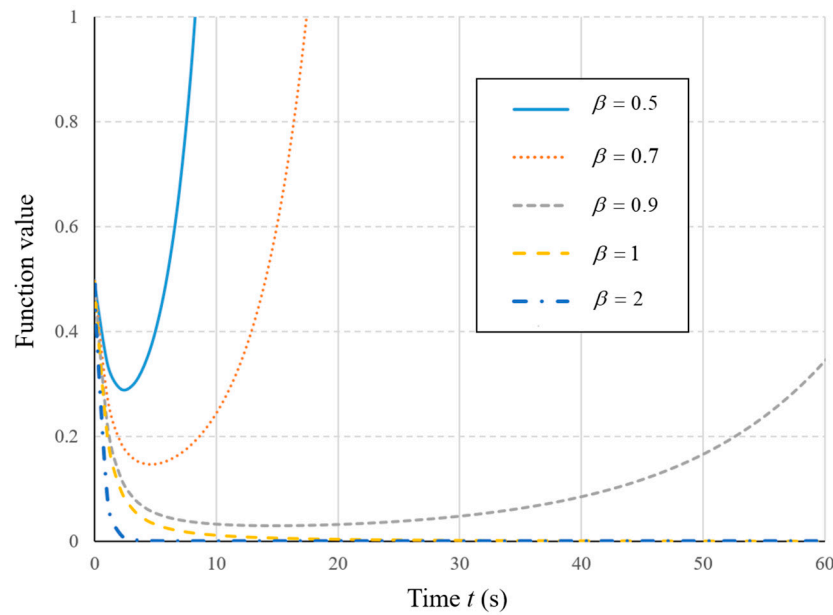
Figure 6. The graphs of the function $\frac{1}{t}\bar{J}_1(t)e^{-\beta t}$ with different values of β.

Therefore, the kernel function of operator $\frac{\sqrt{(p+\beta)^2-\alpha^2}-(p+\beta)}{p}$ could be given:

$$\left[\frac{\sqrt{(p+\beta)^2-\alpha^2}-(p+\beta)}{p}\right]\delta(t) = -\alpha\int_0^t \frac{1}{\tau}\bar{J}_1(\alpha\tau)e^{-\beta\tau}\mathrm{d}\tau. \tag{45}$$

From Equation (45), the kernel function of the operator could be $\frac{1}{p}\sqrt{(p+\beta)^2-\alpha^2}$ derived.

Since $\frac{1}{p}\sqrt{(p+\beta)^2-\alpha^2}$ is an irrational operator, its kernel function is a non-elementary function, given by the integral of the weighted modified Bessel function. If we set $\beta \to 0$ by translation transform, Equation (45) could be reduced to Equation (33).

The convergence of the integral $\int_0^t \frac{1}{\tau}\bar{J}_1(\alpha\tau)e^{-\beta\tau}\mathrm{d}\tau$ is ensured due to the boundedness of the function $\frac{1}{\tau}\bar{J}_1(\alpha\tau)e^{-\beta\tau}$ within the interval $[0,t]$ for any $t > 0$. For the convenience of discussion, we define

$$\int_0^t \frac{1}{\tau}\bar{J}_1(\alpha\tau)e^{-\beta\tau}\mathrm{d}\tau \triangleq \bar{J}_{1e}(-\beta, \alpha t). \tag{46}$$

The modified Bessel function $\bar{J}_1(\alpha\tau)$ is a special function. After applying weighting, $\frac{1}{\tau}\bar{J}_1(\alpha\tau)e^{-\beta\tau}$ is still a special function; therefore, it is reasonable to anticipate that the integral $\bar{J}_{1e}(-\beta, \alpha t)$ should be a new special function.

At last, consider the operator $\frac{1}{\sqrt{p}}\sqrt{(p+\beta)^2-\alpha^2}$. The inverse Laplace transformation gives that

$$\mathcal{L}^{-1}\left(\frac{1}{\sqrt{p}}\right) = \frac{1}{\sqrt{\pi t}}. \tag{47}$$

Equations (39) and (47), combined with the convolution theorem of the Laplace transformation, obtain that

$$\mathcal{L}^{-1}\left[\frac{\sqrt{(p+\beta)^2-\alpha^2}-(p+\beta)}{\sqrt{p}}\right] = -\frac{\alpha}{\sqrt{\pi}}\int_0^t \frac{1}{\sqrt{t-\tau}}\frac{1}{\tau}\bar{J}_1(\alpha\tau)e^{-\beta\tau}\mathrm{d}\tau. \tag{48}$$

The kernel function of the operator in Equation (48) is given as

$$\left[\frac{\sqrt{(p+\beta)^2 - \alpha^2} - (p+\beta)}{\sqrt{p}} \right] \delta(t) = -\frac{\alpha}{\sqrt{\pi}} \int_0^t \frac{1}{\sqrt{t-\tau}} \frac{1}{\tau} \bar{J}_1(\alpha\tau) e^{-\beta\tau} d\tau. \tag{49}$$

The proof of the convergence of the integral $\int_0^t \frac{1}{\sqrt{t-\tau}} \frac{1}{\tau} \bar{J}_1(\alpha\tau) e^{-\beta\tau} d\tau$ could be seen in Appendix B. In Equation (49), the kernel function of operator $\frac{1}{\sqrt{p}}$ is given by Equation (47), and the property of operator $\sqrt{p}$ could be referred to in Courant's work [31]. Therefore, the calculability of the operator $\frac{1}{\sqrt{p}} \sqrt{(p+\beta)^2 - \alpha^2}$ is ensured.

If we let $\beta \to 0$ by translation transform, Equation (49) could be reduced to

$$\left[\frac{\sqrt{p^2 - \alpha^2} - p}{\sqrt{p}} \right] \delta(t) = -\frac{\alpha}{\sqrt{\pi}} \int_0^t \frac{1}{\sqrt{t-\tau}} \frac{1}{\tau} \bar{J}_1(\alpha\tau) d\tau. \tag{50}$$

For the convenience of discussion, we define

$$\int_0^t \frac{1}{\sqrt{t-\tau}} \frac{1}{\tau} \bar{J}_1(\alpha\tau) e^{-\beta\tau} d\tau \triangleq \widetilde{\bar{J}}_{1e}(-\beta, \alpha t). \tag{51}$$

After applying weighting on the Bessel function $\bar{J}_1(\alpha\tau)$, $\frac{1}{\sqrt{t-\tau}} \frac{1}{\tau} \bar{J}_1(\alpha\tau) e^{-\beta\tau}$ is still a special function. It is reasonable to anticipate that the integral $\widetilde{\bar{J}}_{1e}(-\beta, \alpha t)$ should be a new special function.

In the case of $0 < \frac{\beta}{\alpha} < 1$, due to the divergence of the function $\frac{1}{t} \bar{J}_1(t) e^{-\beta t}$, the values of the integrals $\bar{J}_{1e}(-\beta, \alpha t)$ and $\widetilde{\bar{J}}_{1e}(-\beta, \alpha t)$ tends to infinity when $t \to \infty$, indicating poor convergence of the operator and limited practical applicability. Therefore, the following content focuses on the case of $\frac{\beta}{\alpha} \geq 1$.

Suppose that α is fixed as $\alpha = 1$, β is set as $\beta = 1$ and $\beta = 2$, respectively, and the graphs of functions $\bar{J}_{1e}(-\beta, t)$ and $\widetilde{\bar{J}}_{1e}(-\beta, t)$ are shown in Figure 7. The two functions exhibit different monotonicity. The function $\bar{J}_{1e}(-\beta, t)$ tends to a constant value and saturated evolution after monotonically increasing. When $t \to \infty$, there is

$$\lim_{t \to \infty} \bar{J}_{1e}(-1, t) = 1.000, \quad \lim_{t \to \infty} \bar{J}_{1e}(-2, t) = 0.268. \tag{52}$$

The function $\widetilde{\bar{J}}_{1e}(-\beta, t)$ first increases for a short time and then slowly decreases, tending to a constant value. The function $\widetilde{\bar{J}}_{1e}(-1, t)$ attains its maximum value 0.568 at amount $t = 1.1$, and the function $\widetilde{\bar{J}}_{1e}(-2, t)$ attains its maximum value 0.387 at amount $t = 0.45$.

Following the aforementioned analysis, we can obtain that all the kernel functions of the whole operator family in Table 3 exist. It can also be observed that certain operators' kernel functions cannot be directly expressed through established special functions, necessitating the introduction of novel special functions in such cases.

In disciplines such as rock mechanics, the pressure difference often exhibits a gradual decay over time. While exponential and other elementary functions can illustrate the convergence of physical quantities, the convergence is frequently too rapid to accurately represent this slow decay. The gradual decline depicted in Figure 7 suggests that the operator $\frac{1}{\sqrt{p}} \sqrt{(p+\beta)^2 - \alpha^2}$ can effectively characterize this phenomenon.
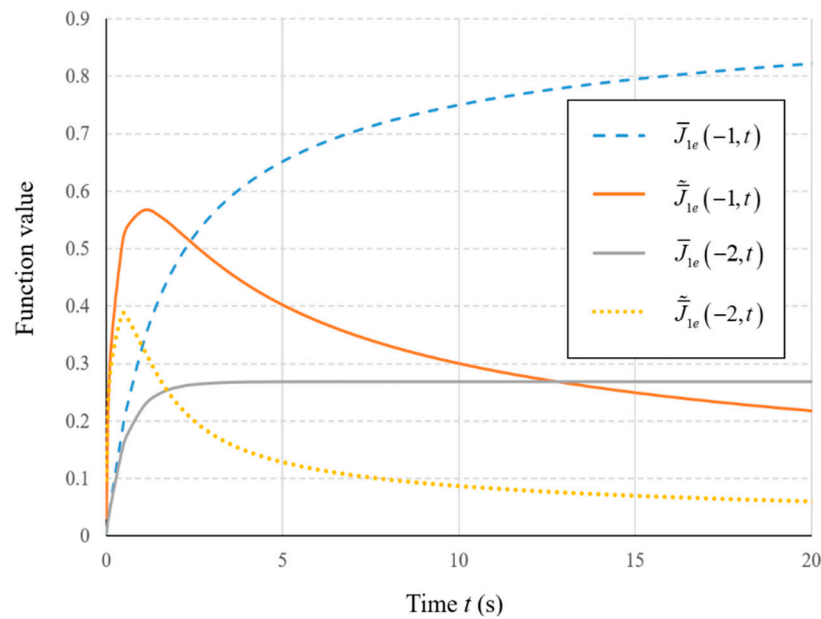
Figure 7. The graphs of functions $\bar{J}_{1e}(-\beta, t)$ and $\tilde{\bar{J}}_{1e}(-\beta, t)$ with different values of β.

5.4. Kernel Functions of the Fractal Operators $\sqrt{(p+\beta)^2 + \alpha^2}$, $\frac{1}{p}\sqrt{(p+\beta)^2 + \alpha^2}$ *and*
$\frac{1}{\sqrt{p}}\sqrt{(p+\beta)^2 + \alpha^2}$

Section 5.1 is symmetric with Section 5.2, and the symmetry can be used for reference. Now that we have Section 5.3, can we construct content that is symmetric with it? The answer is yes. We can construct Section 5.4, the contents of this section.

Extend the parameter α to complex field and introduce the complex transformation

$$\alpha \to i\alpha.$$

Then, the fractal operator $\sqrt{(p+\beta)^2 - \alpha^2} - (p+\beta)$ has the following transformation

$$\sqrt{(p+\beta)^2 - \alpha^2} - (p+\beta) \to \sqrt{(p+\beta)^2 + \alpha^2} - (p+\beta).$$

Based on the above parameter transformation and operator transformation, the content of Section 5.3 can be transformed into the content of this section.

Equation (40) is transformed into

$$\left[\sqrt{(p+\beta)^2 + \alpha^2} - (p+\beta)\right]\delta(t) = -\frac{i\alpha}{t}\bar{J}_1(i\alpha t)e^{-\beta t}. \tag{53}$$

From the transformation between the Bessel function and the modified Bessel function (Equation (25)), we can immediately obtain that

$$\left[\sqrt{(p+\beta)^2 + \alpha^2} - (p+\beta)\right]\delta(t) = \frac{\alpha}{t}J_1(\alpha t)e^{-\beta t}. \tag{54}$$

From Equation (54), the kernel function of the operator $\sqrt{(p+\beta)^2 + \alpha^2}$ could be derived. The comparison between Equation (54) and Equation (40) reveals their complete symmetry, as both the algebraic structure of the operators and the kernel functions exhibit symmetrical characteristics. When $t \to 0$, there is

$$\lim_{t \to 0}\left[\frac{1}{t}J_1(\alpha t)e^{-\beta t}\right] = \frac{\alpha}{2}. \tag{55}$$

When $t \to \infty$, the limit of the kernel function is

$$\lim_{t \to \infty} \left[\frac{1}{t} J_1(\alpha t) e^{-\beta t} \right] = 0. \tag{56}$$

Unlike in Section 5.3, the limit of the kernel function $\frac{1}{t} J_1(\alpha t) e^{-\beta t}$ is not affected by the value of $\frac{\beta}{\alpha}$, as shown in Figure 8. This advantage stems from the inherent oscillation and convergence properties of the Bessel function.
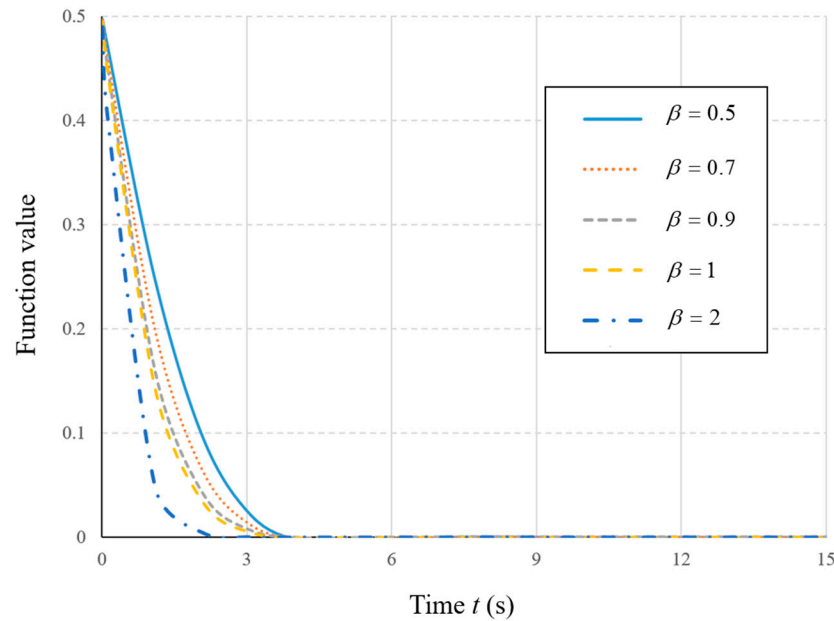

Figure 8. The graphs of the function $\frac{1}{t} J_1(t) e^{-\beta t}$ with different values of β.

In the case of $\frac{\beta}{\alpha} \geq 1$, both functions $\frac{1}{t} J_1(\alpha t) e^{-\beta t}$ and $\frac{1}{t} \overline{J}_1(\alpha t) e^{-\beta t}$ converge rapidly to 0, indicating a high degree of similarity in their graphs. This similarity highlights the inherent symmetry in the fractal operators $\sqrt{(p + \beta)^2 + \alpha^2} - (p + \beta)$ and $\sqrt{(p + \beta)^2 + \alpha^2} - (p + \beta)$.
Similarly, Equations (45) and (49) are transformed into

$$\left[\frac{\sqrt{(p + \beta)^2 + \alpha^2} - (p + \beta)}{p} \right] \delta(t) = \alpha \int_0^t \frac{1}{\tau} J_1(\alpha \tau) e^{-\beta \tau} d\tau, \tag{57}$$

$$\left[\frac{\sqrt{(p + \beta)^2 + \alpha^2} - (p + \beta)}{\sqrt{p}} \right] \delta(t) = \frac{\alpha}{\sqrt{\pi}} \int_0^t \frac{1}{\sqrt{t - \tau}} \frac{1}{\tau} J_1(\alpha \tau) e^{-\beta \tau} d\tau. \tag{58}$$

The proof of the convergence of the integrals at the right side of Equations (57) and (58) is identical to that in Section 5.3. Thus, the calculability of the operators $\frac{\sqrt{(p+\beta)^2+\alpha^2}}{p}$ and $\frac{\sqrt{(p+\beta)^2+\alpha^2}}{\sqrt{p}}$ is ensured.

If we set $\beta \to 0$ by translation transform, Equation (57) could be reduced to Equation (17), and Equation (58) could be reduced to

$$\left[\frac{\sqrt{p^2 + \alpha^2} - p}{\sqrt{p}} \right] \delta(t) = \frac{\alpha}{\sqrt{\pi}} \int_0^t \frac{1}{\sqrt{t - \tau}} \frac{1}{\tau} J_1(\alpha \tau) d\tau. \tag{59}$$

Corresponding to Section 5.3, we have the definitions

$$\int_0^t \frac{1}{\tau} J_1(\alpha\tau) e^{-\beta\tau} d\tau \triangleq J_{1e}(-\beta, \alpha t), \tag{60}$$

$$\int_0^t \frac{1}{\sqrt{t-\tau}} \frac{1}{\tau} J_1(\alpha\tau) e^{-\beta\tau} d\tau \triangleq \widetilde{J}_{1e}(-\beta, \alpha t). \tag{61}$$

Suppose α is fixed as $\alpha = 1$ and β is set to $\beta = 1$ and $\beta = 2$, respectively, and the graphs of functions $J_{1e}(-\beta, t)$ and $\widetilde{J}_{1e}(-\beta, t)$ are shown in Figure 9.
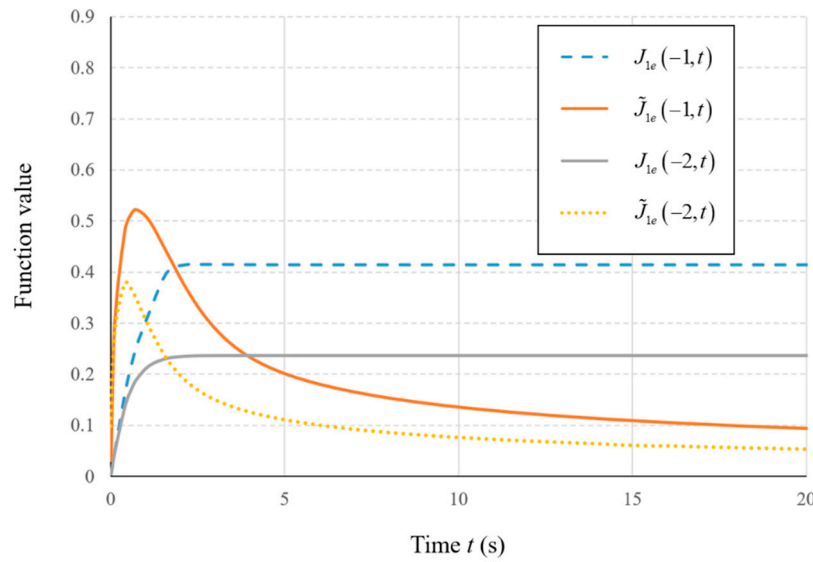
Figure 9. The graphs of functions $J_{1e}(-\beta, t)$ and $\widetilde{J}_{1e}(-\beta, t)$ with different values of β.

By comparing Figures 7 and 9, it can be observed that the graph trends of $J_{1e}(-\beta, t)$ and $\overline{J}_{1e}(-\beta, t)$ are similar, the similarity increasing with the increase of the value of a. The similarity can be attributed to the regulation imposed by the exponential function. This shows that the fractal operators $\frac{\sqrt{(p+\beta)^2+\alpha^2}-(p+\beta)}{p}$ and $\frac{\sqrt{(p+\beta)^2-\alpha^2}-(p+\beta)}{p}$ are symmetric, the symmetry increasing with the increase of the value of β. When $t \to \infty$, there is

$$\lim_{t\to\infty} J_{1e}(-1, t) = 414, \ \lim_{t\to\infty} J_{1e}(-2, t) = 0.236. \tag{62}$$

It can be seen that in the case of $\beta = 2$, the difference between functions $J_{1e}(-2, t)$ and $\overline{J}_{1e}(-2, t)$ is already minimal, and their graph contours are exactly the same.

Similarly, the graph trends of $\widetilde{J}_{1e}(-\beta, t)$ and $\widetilde{\overline{J}}_{1e}(-\beta, t)$ in Figures 7 and 9, respectively, are also similar, which means that the fractal operators $\frac{\sqrt{(p+\beta)^2+\alpha^2}-(p+\beta)}{\sqrt{p}}$ and $\frac{\sqrt{(p+\beta)^2-\alpha^2}-(p+\beta)}{\sqrt{p}}$ also exhibit a pleasing symmetry. The function $\widetilde{J}_{1e}(-1, t)$ attains its maximum value 0.522 at amount $t = 0.75$, and the function $\widetilde{J}_{1e}(-2, t)$ attains its maximum value 0.379 at amount $t = 0.4$. Also, we can see that in the case of $\beta = 2$, the difference between functions $\widetilde{J}_{1e}(-2, t)$ and $\widetilde{\overline{J}}_{1e}(-2, t)$ is already minimal, and their graph contours are exactly the same.

The logical basis of the above symmetries is the symmetry between the Bessel function and the modified Bessel function, as well as the symmetry between the Struve function and the modified Struve function. It is quite an unexpected result.

After comparing Figure 8, Figure 9, and Figure 4, it becomes evident that the oscillation characteristics induced by the Bessel function $J_1(t)$ are completely eradicated following the modulation of $\frac{1}{t} J_1(t) e^{-2t}$, leaving no discernible trace of oscillation on the curve, which

highlights the efficiency of eliminating oscillations by designing parameters with the help of fractal operators.

5.5. Kernel Functions of the Fractal Operators $\sqrt{p + \beta}$, $\frac{1}{p}\sqrt{p + \beta}$ and $\frac{1}{\sqrt{p}}\sqrt{p + \beta}$

$\sqrt{p + \beta}$ is a classical operator. Jian et al. [19] conducted a detailed analysis and derived the following expression:

$$\sqrt{p + \alpha^2}\eta(t) = \alpha\,\mathrm{erf}(\sqrt{\alpha^2 t}) + \frac{e^{-\alpha^2 t}}{\sqrt{\pi t}}, \tag{63}$$

where $\eta(t)$ is the Heaviside step function. Setting $\beta = \alpha^2$ and noting that

$$p\eta(t) = \delta(t), \tag{64}$$

we can give that

$$\frac{1}{p}\sqrt{p + \beta}\,\delta(t) = \sqrt{\beta}\,\mathrm{erf}(\sqrt{\beta t}) + \frac{e^{-\beta t}}{\sqrt{\pi t}}, \tag{65}$$

where $\mathrm{erf}(\cdot)$ is the error function.

The operator $\frac{1}{p}\sqrt{p + \beta}$ will now be considered from a different perspective. When $\beta > 0$, the inverse Laplace transformation gives that

$$\mathcal{L}^{-1}\left(\frac{1}{p}\sqrt{p + \beta}\right) = \frac{e^{-\beta t}}{\sqrt{\pi t}} + \sqrt{\beta}\,\mathrm{erf}\left(\sqrt{\beta t}\right). \tag{66}$$

Therefore, the kernel function of the fractal operator is

$$\frac{1}{p}\sqrt{p + \beta}\,\delta(t) = \frac{e^{-\beta t}}{\sqrt{\pi t}} + \sqrt{\beta}\,\mathrm{erf}\left(\sqrt{\beta t}\right). \tag{67}$$

Equation (67) is consistent with the result derived by Jian et al. [19]. Since $\frac{1}{p}\sqrt{p + \beta}$ is an irrational fractional-type operator, the kernel function contains the non-elementary function $\mathrm{erf}(\cdot)$.

Then, consider the operator $\frac{1}{\sqrt{p}}\sqrt{p + \beta}$. For the Laplace transformation of the modified Bessel function of the first kind $\bar{J}_0$ and $\bar{J}_1$, the following equation is valid:

$$\mathcal{L}\left\{\frac{\beta}{2}\left[\bar{J}_0\left(\frac{\beta t}{2}\right) + \bar{J}_1\left(\frac{\beta t}{2}\right)\right]\right\} = \sqrt{\frac{p + \frac{\beta}{2}}{p - \frac{\beta}{2}}} - 1. \tag{68}$$

Observing the right side of Equation (68), if we introduce the translation transformation, we can obtain that:

$$p \to p + \frac{\beta}{2},$$

Then, we have

$$\sqrt{\frac{p + \frac{\beta}{2}}{p - \frac{\beta}{2}}} \to \sqrt{\frac{p + \beta}{p}}.$$

That is, when the operator p is translated to $p + \frac{\beta}{2}$, the operator is exactly translated to $\sqrt{\frac{p+\beta}{p}}$. Therefore, Equation (68) combined with the translation property of the Laplace transformation obtains that

$$\mathcal{L}\left\{\frac{\beta}{2}e^{-\frac{\beta t}{2}}\left[\bar{J}_0\left(\frac{\beta t}{2}\right) + \bar{J}_1\left(\frac{\beta t}{2}\right)\right]\right\} = \sqrt{\frac{p + \beta}{p}} - 1. \tag{69}$$

It can be derived further that

$$\left[\frac{1}{\sqrt{p}}\sqrt{p+\beta}-1\right]\delta(t) = \frac{\beta}{2}e^{-\frac{\beta t}{2}}\left[\bar{J}_0\left(\frac{\beta t}{2}\right)+\bar{J}_1\left(\frac{\beta t}{2}\right)\right]. \tag{70}$$

$\frac{1}{\sqrt{p}}\sqrt{p+\beta}-1$ is an irrational fractional-type operator, so its kernel function contains the non-elementary function, specifically the modified Bessel function.

6. Conclusions

In this paper, the functional fractal circuit model of arterial blood flow was reconstructed, the fractal operators were abstracted, and their kernel functions were studied. The main conclusions drawn from this are as follows:

1. The structure and motion of living organisms offer abundant resources for exploring new spatial forms and fractal operators. After taking the shunt effect of the branch vessels into account, the reconstructed functional circuit model exhibited a distinct topological structure compared to that of previous models. Such topological structure can indeed yield insightful results.
2. By selecting basic admittance operators, the fractal operator family abstracted from the fractal circuit model constituted the fundamental graph of the apparent 1/2-order operators. The kernel functions and properties of these operators offer novel perspectives on the fields of automatic control and biomechanics.
3. The Bessel function and Struve function were related through explicit integration; the modified Bessel function and modified Struve function also exhibited analogous connection. The connections could be employed for constructing the kernel functions of operators $\frac{1}{p}\sqrt{p^2+\alpha^2}$ and $\frac{1}{p}\sqrt{p^2-\alpha^2}$.
4. By translation transformation, the divergent operators $\sqrt{p^2-\alpha^2}$ and $\frac{1}{p}\sqrt{p^2-\alpha^2}$ were transformed into convergent operators $\sqrt{(p+\beta)^2-\alpha^2}$ and $\frac{1}{p}\sqrt{(p+\beta)^2-\alpha^2}$, greatly broadening the scope of the operators.
5. Under certain conditions, operators $\sqrt{(p+\beta)^2-\alpha^2}$, $\frac{1}{p}\sqrt{(p+\beta)^2-\alpha^2}$, and $\frac{1}{\sqrt{p}}\sqrt{(p+\beta)^2-\alpha^2}$ demonstrate notable symmetry with operators $\sqrt{(p+\beta)^2+\alpha^2}$, $\frac{1}{p}\sqrt{(p+\beta)^2+\alpha^2}$, and $\frac{1}{\sqrt{p}}\sqrt{(p+\beta)^2+\alpha^2}$ respectively. The constructions of the kernel functions for those operators necessitates the introduction of novel special functions, which possess properties challenging to articulate by elementary functions.
6. These results provide a powerful mathematical lexicon and toolkit for the biomechanics.

The results presented in this paper possess broad applicability and can be effectively employed in the fields of biomechanics and automatic control. The scope of this paper is limited to the combination of the fundamental electrical admittance operators: inductance, capacitance, and resistance. To enhance our understanding of biological phenomena, future research will incorporate more intricate electrical components (including fractional-order components) for a more comprehensive depiction.

Data Availability Statement: Data are contained within the article.

Conflicts of Interest: The authors declare no conflicts of interest.

Appendix A. Proof of Equation (19)

The following equation without parameter α is considered first:

$$\left\{ \frac{1}{2} \{ 2[tJ_0(t) - J_1(t)] + \pi t[J_1(t)H_0(t) - J_0(t)H_1(t)] \} \right\}' = \frac{1}{t} J_1(t). \tag{A1}$$

The Bessel function exhibits recursion properties:

$$J'_n(t) = \frac{1}{2} J_{n-1}(t) - \frac{1}{2} J_{n+1}(t), \tag{A2}$$

$$nJ_n(t) = \frac{t}{2} J_{n-1}(t) + \frac{t}{2} J_{n+1}(t). \tag{A3}$$

From Equations (A2) and (A3) we can derive

$$J'_n(t) = \frac{n}{t} J_n(t) - J_{n+1}(t). \tag{A4}$$

The Struve function exhibits recursion properties:

$$H_{n-1}(t) - H_{n+1}(t) = 2H'_n(t) - \frac{1}{\sqrt{\pi}\Gamma\left(n + \frac{3}{2}\right)} \left(\frac{t}{2}\right)^n, \tag{A5}$$

$$H_{n-1}(t) + H_{n+1}(t) = \frac{2n}{t} H_n(t) + \frac{1}{\sqrt{\pi}\Gamma\left(n + \frac{3}{2}\right)} \left(\frac{t}{2}\right)^n. \tag{A6}$$

From Equations (A2), (A4) and (A5), we can derive that

$$J'_0(t) = -J_1(t), \tag{A7}$$

$$J'_1(t) = \frac{1}{2} J_0(t) - \frac{1}{2} J_2(t), \tag{A8}$$

$$H'_0(t) = \frac{1}{2} [H_{-1}(t) + H_1(t)] + \frac{4}{\pi}, \tag{A9}$$

$$H'_1(t) = \frac{1}{2} [H_0(t) + H_2(t)] + \frac{t}{3\pi}. \tag{A10}$$

Substituting Equations (A7)–(A10) into the left side of Equation (A1) obtains

$$\begin{aligned}
&\left\{ \frac{1}{2} \{ J_1(t)[-2 + \pi t H_0(t)] + t J_0(t)[2 - \pi H_1(t)] \} \right\}' \\
&= \frac{1}{2} J_0(t) - \frac{1}{6} t^2 J_0(t) - \frac{1}{2} t J_1(t) + \frac{1}{2} J_2(t) \\
&+ \frac{1}{4} \pi t J_1(t) H_{-1}(t) + \frac{1}{2} \pi J_1(t) H_0(t) \\
&- \frac{1}{4} \pi t J_2(t) H_0(t) - \frac{1}{2} \pi J_0(t) H_1(t) \\
&+ \frac{1}{4} \pi t J_1(t) H_1(t) + \frac{1}{4} \pi t J_0(t) H_2(t)
\end{aligned} . \tag{A11}$$

From Equation (A3), we can obtain that the right side of Equation (A1) satisfies

$$\frac{1}{t} J_1(t) = \frac{1}{2} [J_0(t) + J_2(t)]. \tag{A12}$$

From Equations (A11) and (A12), we can obtain that Equation (A1) is equivalent to the following equation:

$$
\begin{aligned}
&\tfrac{1}{4}\pi J_1(t)H_{-1}(t) + \tfrac{1}{2t}\pi J_1(t)H_0(t) - \tfrac{1}{4}\pi J_2(t)H_0(t) \\
&- \tfrac{1}{2t}\pi J_0(t)H_1(t) + \tfrac{1}{4}\pi J_1(t)H_1(t) + \tfrac{1}{4}\pi J_0(t)H_2(t) \\
&= \tfrac{t}{6}J_0(t) + \tfrac{1}{2}J_1(t)
\end{aligned} \tag{A13}
$$

Then, we only need to prove Equation (A13). Substituting Equation (A12) into the left side of the Equation (A13); eliminating $\frac{1}{t}J_1(t)$, (A13) changes into

$$
\begin{aligned}
&\tfrac{1}{4}\pi J_1(t)H_{-1}(t) + \tfrac{1}{4}\pi J_0(t)H_0(t) \\
&- \tfrac{1}{2t}\pi J_0(t)H_1(t) + \tfrac{1}{4}\pi J_1(t)H_1(t) \\
&+ \tfrac{1}{4}\pi J_0(t)H_2(t) \\
&= \tfrac{t}{6}J_0(t) + \tfrac{1}{2}J_1(t)
\end{aligned} \tag{A14}
$$

From Equation (A6) we can obtain that

$$
H_0(t) + H_2(t) = \frac{2}{t}H_1(t) + \frac{2t}{3\pi}, \tag{A15}
$$

$$
H_{-1}(t) + H_1(t) = \frac{2}{\pi}. \tag{A16}
$$

Substituting Equation (A15) into Equation (A14), eliminating $H_0(t) + H_2(t)$, Equation (A14) changes into

$$
\frac{1}{4}\pi J_1(t)H_{-1}(t) + \frac{1}{4}\pi J_1(t)H_1(t) + \frac{1}{6}tJ_0(t) = \frac{t}{6}J_0(t) + \frac{1}{2}J_1(t). \tag{A17}
$$

Substituting Equation (A16) into the left side of Equation (A17) directly obtains the right side of Equation (A17); therefore, Equation (A17) is valid, i.e., the Equation (A1) is valid.

In Equation (A1), substituting the variable t into αt, i.e.,

$$
t \to \alpha t,
$$

we can obtain that

$$
\frac{d}{d(\alpha t)}\left\{\frac{1}{2}\{2[\alpha t J_0(\alpha t) - J_1(\alpha t)] + \pi \alpha t[J_1(\alpha t)H_0(\alpha t) - J_0(\alpha t)H_1(\alpha t)]\}\right\} = \frac{1}{\alpha t}J_1(\alpha t), \tag{A18}
$$

i.e.,

$$
\frac{d}{dt}\left\{\frac{1}{2}\{2[\alpha t J_0(\alpha t) - J_1(\alpha t)] + \pi \alpha t[J_1(\alpha t)H_0(\alpha t) - J_0(\alpha t)H_1(\alpha t)]\}\right\} = \frac{1}{t}J_1(\alpha t). \tag{A19}
$$

The Equation (A19) is obviously equivalent to Equation (19); therefore, Equation (19) is proved.

Appendix B. Proof of the Convergence of the Integral $\int_0^t \frac{1}{\tau\sqrt{t-\tau}}\bar{J}_1(\alpha\tau)e^{-\beta\tau}d\tau$

The theorem of convergence for improper integrals is introduced:

Theorem A1. *Suppose that the function $f(x)$ is continuous over the interval $(a, b]$, and there is $f(x) \geq 0$, and $x = a$ is a flaw of $f(x)$. If there exists $0 < q < 1$, which makes the limit $\lim\limits_{x \to a^+}(x - a)^q f(x)$ exist; then, the improper integral $\int_a^b f(x)dx$ is convergent.*

In the integral $\int_0^t \frac{1}{\tau\sqrt{t-\tau}}\bar{J}_1(\alpha\tau)e^{-\beta\tau}\mathrm{d}\tau$, introduce the variable substitution $\zeta = -\tau$; then, we have

$$
\begin{aligned}
&\int_0^t \frac{1}{\sqrt{t-\tau}}\frac{1}{\tau}\bar{J}_1(\alpha\tau)e^{-\beta\tau}\mathrm{d}\tau \\
&= \int_0^t \frac{1}{\sqrt{t+(-\tau)}}\frac{1}{\tau}\bar{J}_1(\alpha\tau)e^{\beta(-\tau)}\mathrm{d}\tau \\
&= \int_0^{-t} \frac{1}{\sqrt{t+\zeta}}\frac{1}{(-\zeta)}\bar{J}_1(-\alpha\zeta)e^{\beta\zeta}\mathrm{d}(-\zeta) \\
&= \int_{-t}^0 \frac{1}{\sqrt{t+\zeta}}\frac{1}{\zeta}\bar{J}_1(\alpha\zeta)e^{\beta\zeta}\mathrm{d}\zeta
\end{aligned}
\tag{A20}
$$

We have $\alpha, \beta > 0$, and $t > 0$, so there is $\frac{1}{\zeta\sqrt{t+\zeta}}\bar{J}_1(\alpha\zeta)e^{\beta\zeta} \geq 0$ over the interval $-t < \zeta < 0$. Obviously, $\zeta = -t$ is the flaw of the integrand. At $\zeta = 0$, the limit of the integrand is $\lim\limits_{\zeta\to 0}\frac{1}{\sqrt{t+\zeta}}\frac{1}{\zeta}\bar{J}_1(\alpha\zeta)e^{\beta\zeta} = \frac{\alpha}{2\sqrt{t}}$, i.e., the limit exists. Therefore, the case at $\zeta = 0$ does not affect the convergence of the entire integral. Based on the fact that

$$
\begin{aligned}
&\lim\limits_{\zeta\to(-t)^+}(\zeta+t)^{\frac{1}{2}}\frac{1}{\sqrt{t+\zeta}}\frac{1}{\zeta}\bar{J}_1(\alpha\zeta)e^{\beta\zeta} \\
&= \lim\limits_{\zeta\to(-t)^+}\frac{1}{\zeta}\bar{J}_1(\alpha\zeta)e^{\beta\zeta} \\
&= \frac{1}{t}\bar{J}_1(\alpha t)e^{-\beta t}
\end{aligned}
\tag{A21}
$$

the limit $\lim\limits_{\zeta\to(-t)^+}(\zeta+t)^{\frac{1}{2}}\frac{1}{\sqrt{t+\zeta}}\frac{1}{\zeta}\bar{J}_1(\alpha\zeta)e^{\beta\zeta}$ exists. Then according to the Theorem, the integral $\int_{-t}^0 \frac{1}{\sqrt{t+\zeta}}\frac{1}{\zeta}\bar{J}_1(\alpha\zeta)e^{\beta\zeta}\mathrm{d}\zeta$ is convergent, i.e., the integral $\int_0^t \frac{1}{\tau\sqrt{t-\tau}}\bar{J}_1(\alpha\tau)e^{-\beta\tau}\mathrm{d}\tau$ is convergent.

References

1. Hales, S. *Statical Essays: Containing Haemostaticks*; Innys and Manby: London, UK, 1733.
2. Frank, O. Die grundform des arteriellen pulses. *Ztg. Biol.* **1899**, *37*, 483–586.
3. Goldwyn, R.M.; Watt, T.B. Arterial pressure pulse contour analysis via a mathematical model for the clinical quantification of human vascular properties. *IEEE Trans. Biomed. Eng.* **1967**, *BME-14*, 11–17. [CrossRef]
4. Burattini, R.; Gnudi, G. Computer identification of models for the arterial tree input impedance: Comparison between two new simple models and first experimental results. *Med. Biol. Eng. Comput.* **1982**, *20*, 134–144. [CrossRef] [PubMed]
5. Stergiopulos, N.; Westerhof, B.E.; Westerhof, N. Total arterial inertance as the fourth element of the windkessel model. *Am. J. Physiol.-Heart C* **1999**, *276*, H81–H88. [CrossRef] [PubMed]
6. Jager, G.N.; Westerhof, N.; Noordergraaf, A. Oscillatory flow impedance in electrical analog of arterial system: Representation of sleeve effect and non-Newtonian properties of blood. *Circ. Res.* **1965**, *16*, 121–133. [CrossRef] [PubMed]
7. Westerhof, N.; Elzinga, G.; Sipkema, P. An artificial arterial system for pumping hearts. *J. Appl. Physiol.* **1971**, *31*, 776–781. [CrossRef] [PubMed]
8. Shim, Y.T.; Pasipoularides, A.; Straley, C.A.; Hampton, T.G.; Soto, P.F.; Owen, C.H.; Davis, J.W.; Glower, D.D. Arterial windkessel parameter estimation: A new time-domain method. *Ann. Biomed. Eng.* **1994**, *22*, 66–77. [CrossRef] [PubMed]
9. Mandeville, J.B.; Marota, J.J.A.; Ayata, C.; Zaharchuk, G.; Moskowitz, M.A.; Rosen, B.R.; Weisskoff, R.M. Evidence of a cerebrovascular postarteriole Windkessel with delayed compliance. *J. Cereb. Blood Flow Metab.* **1999**, *19*, 679–689. [CrossRef]
10. Rupnic, M.; Runvovc, F. Simulation of steady state and transient phenomena by using the equivalent electronic circuit. *Comput. Meth. Programs Biomed.* **2002**, *67*, 1–12. [CrossRef]
11. Abdolrazaghi, M.; Navidbakhsh, M.; Hassani, K. Mathematical modelling of intra-aortic balloon pump. *Comput. Methods Biomech. Biomed. Eng.* **2010**, *13*, 567–576. [CrossRef]
12. Gul, R.; Schütte, C.; Bernhard, S. Mathematical modeling and sensitivity analysis of arterial anastomosis in the arm. *Appl. Math. Model.* **2016**, *40*, 7724–7738. [CrossRef]
13. Baker, W.B.; Parthasarathy, A.B.; Gannon, K.P.; Kavuri, V.C.; Busch, D.R.; Abramson, K.; He, L.; Mesquita, R.C.; Mullen, M.T.; Detre, J.A.; et al. Noninvasive optical monitoring of critical closing pressure and arteriole compliance in human subjects. *J. Cereb. Blood Flow Metab.* **2017**, *37*, 2691–2705. [CrossRef]
14. Li, B.; Mao, B.Y.; Feng, Y.; Liu, J.C.; Zhao, Z.; Duan, M.Y.; Liu, Y.J. The hemodynamic mechanism of FFR-guided coronary arterybypass grafting. *Front. Physiol.* **2021**, *12*, 8.

15. Nichols, W.W.; Conti, C.R.; Walker, W.E.; Milnor, W.R. Input impedance of the systemic circulation in man. *Circ. Res.* **1971**, *40*, 451–458. [CrossRef]

16. Packard, R.R.S.; Luo, Y.; Abiri, P.; Jen, N.; Aksoy, O.; Suh, W.M.; Tai, Y.C.; Hsiai, T.K. 3-D Electrochemical Impedance Spectroscopy Mapping of Arteries to Detect Metabolically Active but Angiographically Invisible Atherosclerotic Lesions. *Theranostics* **2017**, *7*, 2431–2442. [CrossRef] [PubMed]

17. Guo, J.Q.; Yin, Y.J.; Ren, G.X. Abstraction and operator characterization of fractal ladder viscoelastic hyper-cell for ligaments and tendons. *Appl. Math. Mech.* **2019**, *40*, 1429–1448. [CrossRef]

18. Guo, J.Q.; Yin, Y.J.; Hu, X.L.; Ren, G.X. Self-similar network model for fractional-order neuronal spiking: Implications of dendritic spine functions. *Nonlinear Dynam* **2020**, *100*, 921–935. [CrossRef]

19. Jian, Z.M.; Peng, G.; Li, D.A.; Yu, X.B.; Yin, Y.J. Correlation between Convolution Kernel Function and Error Function of Bone Fractal Operators. *Fractal Fract.* **2023**, *7*, 707. [CrossRef]

20. Peng, G.; Guo, J.Q.; Yin, Y.J. Self-Similar Functional Circuit Models of Arteries and Deterministic Fractal Operators: Theoretical Revelation for Biomimetic Materials. *Int. J. Mol. Sci.* **2021**, *22*, 12897. [CrossRef]

21. Yin, Y.J.; Guo, J.Q.; Peng, G.; Yu, X.B.; Kong, Y.Y. Fractal Operators and Fractional Dynamics with 1/2 Order in Biological Systems. *Fractal Fract.* **2022**, *6*, 378. [CrossRef]

22. Yin, Y.J.; Peng, G.; Yu, X.B. Algebraic equations and non-integer orders of fractal operators abstracted from biomechanics. *Acta Mech. Sin.* **2022**, *38*, 521488.

23. Colombaro, I.; Garra, R.; Giusti, A.; Mainardi, F. Scott-Blair models with time-varying viscosity. *Appl. Math. Lett.* **2018**, *86*, 57–63. [CrossRef]

24. Zhou, H.W.; Wang, C.P.; Han, B.B.; Duan, Z.Q. A creep constitutive model for salt rock based on fractional derivatives. *Int. J. Rock Mech. Min. Sci.* **2011**, *48*, 116–121. [CrossRef]

25. Yin, D.S.; Zhang, W.; Cheng, C.; Li, Y.Q. Fractional time-dependent Bingham model for muddy clay. *J. Non-Newton. Fluid Mech.* **2012**, *187*, 32–35. [CrossRef]

26. Westerhof, N. *Snapshots of Hemodynamics an Aid for Clinical Research and Graduate Education*, 3rd ed.; Springer International Publishing: Cham, Switzerland, 2019.

27. Mandelbrot, B.B.; Aizenman, M. Fractals: Form, Chance, and Dimension. *Phys. Today* **1979**, *32*, 65–66. [CrossRef]

28. Feder, J. *Fractals*; Plenum Press: New York, NY, USA, 1988.

29. Mikusinski, J. *Operational Calculus*, 2nd ed.; Pergamon Press: Oxford, UK, 1983.

30. Yu, X.B.; Yin, Y.J. Operator Kernel Functions in Operational Calculus and Applications in Fractals with Fractional Operators. *Fractal Fract.* **2023**, *7*, 755. [CrossRef]

31. Heaviside, O. On Operators in Physical Mathematics, Part I. *Proc. R. Soc. Lond. Ser. A-Math. Phys. Eng. Sci.* **1893**, *52*, 315–320.

32. Courant, R.; Hilbert, D. *Methods of Mathematical Physics*; Interscience Publishers: New York, NY, USA, 1962.

33. Milnor, W.R. *Hemodynamics*, 2nd ed.; William & Wilkins: Baltimore, MD, USA, 1989.

34. Screen, H.R.C. Investigating load relaxation mechanics in tendon. *J. Mech. Behav. Biomed. Mater.* **2008**, *1*, 51–58. [CrossRef]

35. Shen, Z.L.; Kahn, H.; Ballarini, R.; Eppell, S.J. Viscoelastic properties of isolated collagen fibrils. *Biophys. J.* **2011**, *100*, 3008–3015. [CrossRef]

36. Joglekar, M.R.; Mejias, J.F.; Yang, G.R.; Wang, X.J. Inter-areal balanced amplification enhances signal propagation in a large-scale circuit model of the primate cortex. *Neuron* **2018**, *98*, 222–234.e8. [CrossRef]

37. Chaudhuri, R.; Knoblauch, K.; Gariel, M.A.; Kennedy, H.; Wang, X.J. A large-scale circuit mechanism for hierarchical dynamical processing in the primate cortex. *Neuron* **2015**, *88*, 419–431. [CrossRef] [PubMed]

38. Abramowitz, M.; Stegun, I.A. *Handbook of Mathematical Functions with Formulas, Graphs, and Mathematical Tables*; Dover Publications: New York, NY, USA, 1972.

39. Dai, Z.; Peng, Y.; Mansy, H.A.; Sandler, R.H.; Royston, T.J. A model of lung parenchyma stress relaxation using fractional viscoelasticity. *Med. Eng. Phys.* **2015**, *37*, 752–758. [CrossRef] [PubMed]

40. Craiem, D.; Rojo, F.J.; Atienza, J.M.; Armentano, R.L.; Guinea, G.V. Fractional-order viscoelasticity applied to describe uniaxial stress relaxation of human arteries. *Phys. Med. Biol.* **2008**, *53*, 4543. [CrossRef] [PubMed]